Journal of Molecular Liquids 391 (2023) 123263

Contents lists available at ScienceDirect

Journal of Molecular Liquids

journal homepage: www.elsevier.com/locate/molliq

Tailoring the physical properties of non-isocyanate polyurethanes by introducing secondary amino groups along their main chain

Izabela Łukaszewska [a,*], Sebastian Lalik [b], Artur Bukowczan [a], Monika Marzec [b], Krzysztof Pielichowski [a], Konstantinos N. Raftopoulos [a]

[a] Department of Chemistry and Technology of Polymers, Cracow University of Technology, Warszawska 24, 31-155 Kraków, Poland
[b] Institute of Physics, Jagiellonian University, Prof. S. Łojasiewicza 11, 30-348 Kraków, Poland

ARTICLE INFO

Keywords:
Non-isocyanate polyurethanes
Hydrogen bonding
Molecular mobility

ABSTRACT

A series of linear non-isocyanate polyhydroxyurethanes (NIPUs) were synthesized by aminolysis of a PPO biscyclic carbonate with two diamines, one of which (triethylenetetramine, TETA) contains non-reacting secondary amino groups. Thus, varying the composition of the diamine component modulates the density of proton donors. Fourier Transform Infrared Spectroscopy (FTIR) showed that with increasing TETA content in the amine components (20–100 wt%) carbonyl groups tend to form progressively more double hydrogen bonds (HBs). Interestingly, the system without this amine deviates from the trend. In the whole composition range, a higher amount of double HBs correlates monotonously with reduced molecular mobility as observed by differential scanning calorimetry (DSC), dielectric relaxation spectroscopy (DRS), and dynamic mechanical analysis (DMA). It also correlates with the mechanical properties of studied NIPUs which range at room temperature from a viscous liquid to a dimensionally stable, flexible, and durable elastomer, depending on the density of double hydrogen-bonded carbonyls. Hence, the herein proposed approach allows for tailoring thermomechanical properties of NIPUs by modulating density of double hydrogen-bonded carbonyls.

1. Introduction

Polyurethanes (PUs) are a group of polymeric materials that found a wide range of applications – from construction, through automotive and furniture to biomedicine. The versatility of polyurethanes results primarily from the possibility of adjusting their form and tailoring their properties through appropriate selection of components [1]. Despite the many advantages, there are also some risks associated with the use of conventional polyurethanes. These risks mainly derive from using isocyanates as raw materials for their synthesis. It has been established that isocyanates are harmful not only as monomers, but also through all stages of the polymers life-cycle. Moreover the synthesis of isocyanates involves the use of phosgene, which is a toxic and explosive gas [2].

Thus, in recent years much attention has been paid to the development of more environment-friendly methods for the synthesis of polyurethanes through non-isocyanate routes. The most promising method for the synthesis of non-isocyanate polyurethanes (NIPUs) seems to be aminolysis of cyclic carbonates (CCs), which leads to formation of poly (hydroxy urethanes) (PHUs, H-NIPUs). This procedure not only eliminates the usage of phosgene, isocyanates, acyl chlorides and chloroformates, but also enables utilization of CO_2 since cyclic carbonates might be obtained by addition of carbon dioxide to oxirane ring [3].

Interestingly, polyaddition of amines and cyclic carbonates leads to products with additional advantages. Withdrawal from isocyanates leads to absence of thermally labile allophanate and biuret groups that might be formed during synthesis of conventional polyurethanes. Therefore, non-isocyanate polyurethanes (NIPUs) tend to exhibit superior thermal stability [4]. Attention should be paid that the above might not be true if secondary reaction lead to ureas formation [5]. A second advantage is that hydroxyl groups that are formed alongside urethane groups during cyclic carbonates aminolysis lead to better hydrolytic stability of NIPUs as compared to conventional polyurethanes. Hydroxyl groups present next to the urethanes form not only intermolecular hydrogen bonds, but also intramolecular ones that protect the carbonyl carbon in the urethane group. As a consequence, PHUs exhibit superior hydrolytic stability in comparison with conventional polyurethanes [3].

Functionality and structure of reagents strongly influence properties of the final NIPUs. Polyaddition of rigid biscyclic carbonates and

* Corresponding author.
E-mail address: izabela.lukaszewska@doktorant.pk.edu.pl (I. Łukaszewska).

https://doi.org/10.1016/j.molliq.2023.123263
Received 30 March 2023; Received in revised form 11 September 2023; Accepted 5 October 2023
Available online 6 October 2023

polyamines yields brittle and rigid NIPUs [6]. Using trifunctional carbonates allows for formation of thermosets with good mechanical properties [7], while using hyperbranched polyamines and hydrophilic cyclic carbonates (e.g. CCs based on PEG chain) [8] or diamines and hyperbranched cyclic carbonates [9] allows to obtain NIPU hydrogels of inferior mechanical properties as compared to abovementioned thermosets. Samata *et al.* [10] showed that the shorter carbon chain length of aliphatic amines used as chain extenders, the higher glass transition of final NIPUs since shorter chain extenders provide higher urethane group densities along the polymer chain, and allow for higher density of cross-links if multifunctional raw materials are used. As reported by Zhang *et al.* amine structure influences solubility of PHUs with isophorone diamine affording NIPUs of superior solubility in DMF compared to analogue NIPUs based on aliphatic amines [11]. The type of used amine influences the molecular weights of final polymers as well. Aliphatic linear amines, such as 1,6-hexanediamine, yield NIPUs of higher average molecular masses compared to NIPUs based on isophorone diamine, which is attributed to steric hindrances present for non-linear amines. Using linear amines results in NIPUs with lower glass transition temperatures in comparison to cycloaliphatic amines due to the rigidness of the latter ones [11].

Presence of other functional groups alongside CC chain or amine chain may also impact properties of non-isocyanate polyurethanes. Ester groups present in cyclic carbonate chain may undergo reaction with amine groups, which leads to formation of amides and polyol by-products and may result in plasticization of NIPUs as well as undesirable emissions of low-molecular compounds [6,12].

Current findings focus on the influence of amine structure on NIPU properties in regard to differences in amines' carbon chain architectures, e.g. chain length or presence of aliphatic rings. Another factor that influences the physical properties of polymers is hydrogen bonding [13], especially in biological systems and biomaterials, in which hydrogen bonds govern supramolecular ordering [14], allowing to tailor materials' properties or even to introduce new ones, e.g. self-healing or injectability [15]. However, not much attention has been paid to the possibility of tailoring NIPU properties by modulating hydrogen bonding density or nature.

We expect that introducing additional hydrogen bond donor groups will have a significant impact on the properties of NIPUs, due to increasing hydrogen bond density. In this paper we focus on determining the influence of secondary amino groups as hydrogen bond donors along the main polymeric chain, on the density and nature of hydrogen bonding in poly(hydroxy urethanes), and its subsequent impact on the chain mobility and mechanical performance of NIPUs.

For this reason, we synthesized a series of linear poly(hydroxy urethanes) using two types of linear diamines, namely triethylenetetramine (TETA) and 1,4-diaminobutane (DAB). TETA possesses two secondary amino groups along its contour, while DAB lacks such moieties. By varying the mass ratio of the diamines we modulated the amount of proton donors in the system, and studied in detail its effect on the hydrogen bonding of the carbonyl groups. We will show that the resulting hydrogen bonding is very strongly correlated with the thermal and dynamic glass transition, as well as with the mechanical properties of the NIPU materials.

2. Experimental

2.1. Materials

PPO Bis carbonate (CC, M_w ~ 480 g/mol) was purchased from Specific Polymers (Castries, France). Triethylenetetraamine (TETA), 1,4-diaminobutane (DAB), 1,5,7-Triazabicyclodec-5-ene (TBD) were purchased from Sigma-Aldrich (Darmstadt, Germany). Dimethylacetamide (purity 97 %) was purchased from Pol-Aura (Zabrze, Poland). All materials were used as received. The structures of used pristine compounds are shown in Supplementary Material (Figure S1).

2.2. Synthesis

2.2.1. Synthesis of PHUs

Non-isocyanate polyurethanes based on two-amines were synthesized using a two-step method (Scheme 1). The reaction was carried out at 60 °C in argon atmosphere under a reflux condenser. During the first step, pre-calculated amounts of the PPO-based biscyclic carbonate (CC), triethylenetetramine (TETA), dimethylacetamide (DMAc), and the (TBD) as a catalyst were added to a flask to form carbonate terminated TETA segments. The mixture was stirred at 300 rpm with a magnetic stirrer. The progress of the reaction was monitored by following changes in FTIR spectra of the reaction mixture (Fig. 1). An aliquot was removed from the flask every 24 h and a spectrum was recorded as described in 2.3.1. Once there were no observable changes in bands assigned to stretching vibrations of carbonyls in cyclic carbonate ring (1800 cm^{-1}) and stretching vibrations of carbonyls in urethane groups (1700 cm^{-1}) [16], the first step was considered complete. FTIR spectra of reaction mixture also show gradual formation of hydroxyl groups (stretching vibrations at 3300 cm^{-1}) [17] during aminolysis of cyclic carbonates which indicates formation of hydroxy-urethane groups.

In the second step a pre-calculated amount of DAB was added to the flask and the mixture was stirred at 300 rpm to form the final copolymer. Mixing continued until no further changes in the carbonyl band of cyclic carbonate (1800 cm^{-1}) was observed (approx. 3 h). The mixture was then poured into a polypropylene mold and dried at 90 °C under vacuum until DMAc was evaporated.

Non-isocyanate polyurethanes based on one-amine system were synthesized via one-step route in which all components were added to the flask at the beginning of the reaction. All other parameters and procedures remained unchanged.

Finally, seven materials were synthesized, with TETA content in the amine reagent ranging from 0 to 100 wt%. The obtained products were labelled according to mass fraction of TETA in the amine component, e.g. T50 stands for the material with 50 wt% of TETA in the amine component. The amine component mass was 1.5 g for all the materials. Cyclic carbonate (CC) mass was equimolar to the amine component, assuming that only primary amine groups react. Secondary amine groups were considered unreactive under given conditions, an assumption for which we provide argumentation and evidence in the Supplementary Material (Section B).

It is noteworthy that due to its larger molar mass, the cyclic carbonate is the main 'mass contributor', while amine component constituted only ~ 20 % of the mass of the final product (Figure S3 in Supplementary Material). Yet, as will be shown in this article, the type of used amine strongly influences thermal and mechanical properties of NIPU, as well as determines materials structural integrity and state. Varying TETA content in amine reagents allowed for obtaining NIPUs in a form of either a viscous liquid, very soft solid, brittle solid, or a durable elastomer mechanically stable even in high temperatures. This was the first indication that in materials at hand hydrogen bonding plays the crucial role in determining physical properties, and that modulating the density of hydrogen bonds is a key factor to tailor NIPUs properties. In addition, preliminary DSC runs up to 200 °C (Figure S4 in Supplementary Material) showed no crystallization nor any order to disorder transitions as is usually observed in conventional polyurethanes in this region. Thus, the materials should be considered fully amorphous.

2.3. Methods

2.3.1. Fourier transform infrared spectroscopy (FTIR)

Fourier-transform infrared spectroscopy (FTIR) analysis was carried out using a Thermo Scientific Nicolet iS5 spectrometer equipped with the iD7 ATR Accessory with diamond crystal prism, in a wavenumber range 4000–400 cm^{-1}, with a scanning resolution of 4 cm^{-1}, data gap 0.482 cm^{-1}, and 16 scans averaged at each measurement.

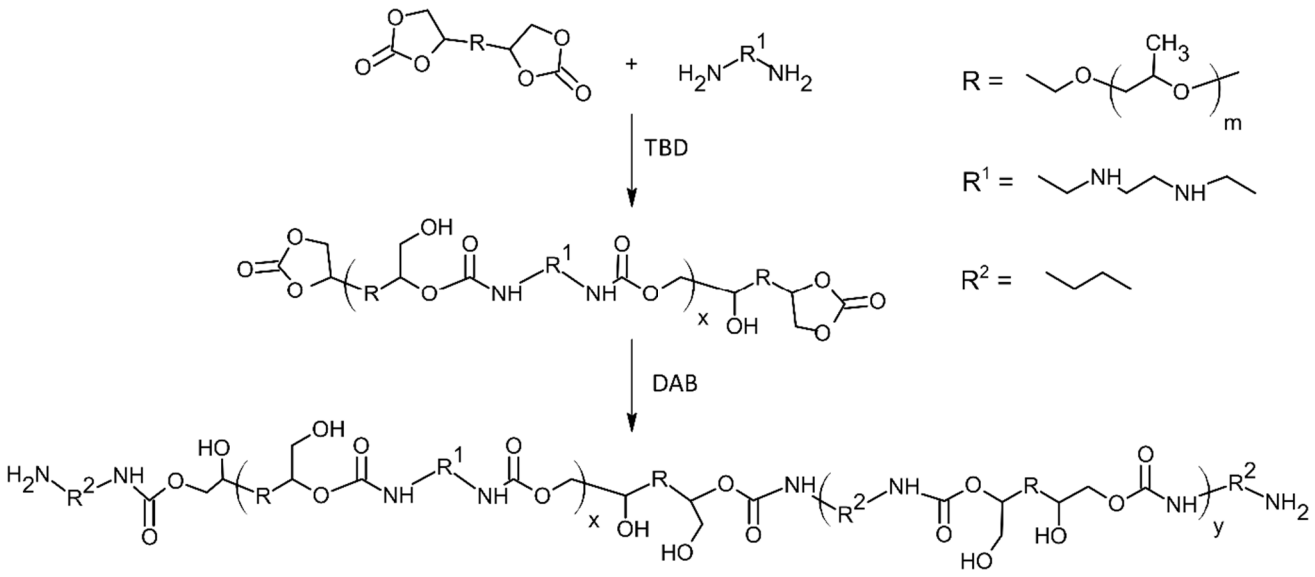

Scheme 1. Scheme of two step cyclic carbonate aminolysis.

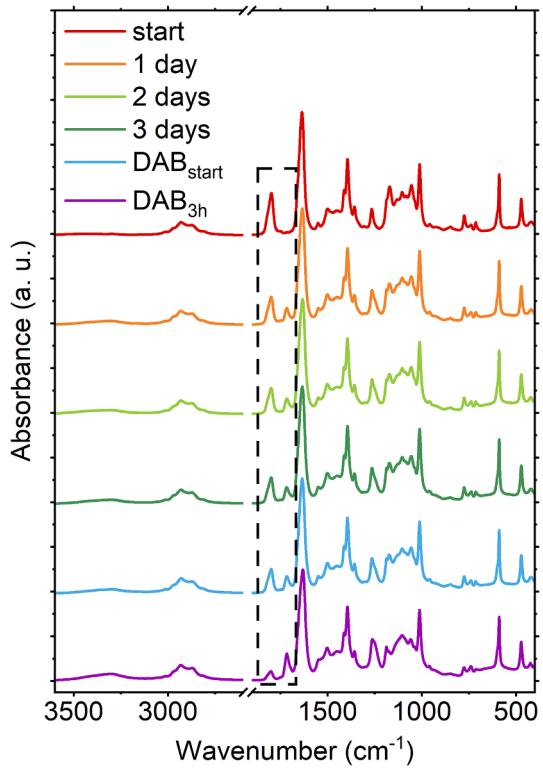

Fig. 1. FTIR spectra of reaction mixture of T60 material recorded: after mixing of carbonate, solvent, catalyst, and TETA (start); during the first step of the synthesis after 24, 48, and 72 h; during the second step of synthesis: after introduction of DAB to the system (DAB_{start}) and after 3 h (DAB_{3h}). Region of monitored changes is marked with a dashed box.

2.3.2. Differential scanning calorimetry (DSC)

DSC experiments were carried out with a Mettler Toledo 823e differential scanning calorimeter purged with argon. Samples of 5–6 mg were dried over phosphorus pentoxide until equilibrium, and then measured in the temperature range − 85 °C to 70 °C, at rate 10 K/min. The values of glass transition temperatures T_g were calculated as midpoint of the endothermic step.

2.3.3. Dynamic mechanical analysis (DMA)

Dynamic Mechanical Analysis (DMA) was performed using a DMA 242C Netzsch apparatus in tension mode. Prior to measurements, samples of approx. cross-section 0.5x4.0 mm and length 7.0 mm were dried over phosphorus pentoxide until equilibrium. Measurements were carried out under nitrogen atmosphere using liquid nitrogen as cooling medium with heating rate of 2 K/min, frequency of 5 Hz and maximal dynamic force of 4 N.

2.3.4. Broadband dielectric spectroscopy (BDS)

Samples were dried over phosphorous pentoxide, until equilibration of their mass. Then dielectric spectra were recorded during step-wise heating from −100 °C up to 90 °C, at steps of 5 or 10 K in the frequency range of 100 mHz – 5 MHz and measuring voltage of 1.0 V. The spectra were recorded by a Turnkey Impedance Spectrometer Concept 81 (Novocontrol Technologies GmbH & Co. KG). Accuracy of temperature was better than 0.5 K. Brass electrodes of diameter 9.60 mm and thickness 2.50 mm were used to measure samples of thickness 0.5–1.0 mm.

3. Results and discussion

3.1. Chemical structure – Fourier transform infrared spectroscopy

Fig. 2a shows FTIR spectra of the final materials. Bands at 1800 cm^{-1} associated with carbonyl stretching in CC ring [18] disappear almost completely indicating high conversion rate of the reaction. The differences of intensities of aforementioned bands between samples are small and are believed to not affect significantly physical properties of the final materials. Simultaneously, pronounced bands at 3300–3500 cm^{-1} correspond to stretching vibrations of hydroxyl/amine groups, and those around 1700 cm^{-1} are associated with stretching vibrations of carbonyls in urethanes [5]. Those bands, alongside the one at 1370 cm^{-1} (C-N stretching vibrations in urethanes), and at 1530 cm^{-1} (bending vibrations of N–H and C-N in urethanes), confirm formation of poly (hydroxy urethanes) [19–21]. The carbonyl region exhibits a complex structure and is discussed more extensively later in this paper, as it is suitable for the study of hydrogen bonding in the system.

The bands at 2860 cm^{-1} and 2960 cm^{-1}, corresponding to symmetric and asymmetric $–CH_2$ stretching vibrations respectively, overlap with stretching vibrations of $–CH_3$ groups at 2950 cm^{-1} [22]. Bands in this aliphatic stretching region are not significantly affected by the

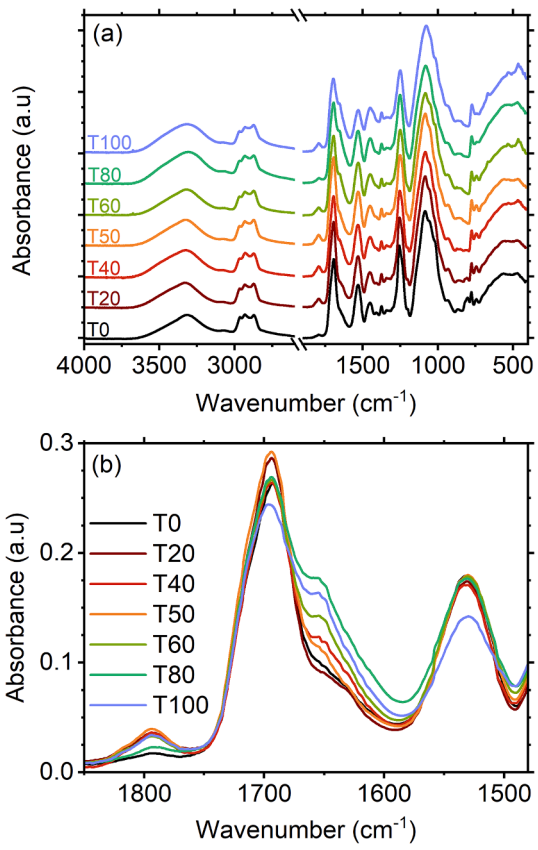

Fig. 2. (a) FTIR spectra of dry NIPUs. The curves have been translated for clarity; (b) FTIR spectra in the carbonyl stretching region.

composition of the amine component. The bands at wavenumber range 1150 cm^{-1} to 1030 cm^{-1} are associated with the asymmetric stretching vibrations of the C-O-C bonds along the PPO chain, which originates from cyclic carbonate [23].

3.1.1. *Carbonyl region – Hydrogen bonding*

The most suitable band for the study of hydrogen bonding is the carbonyl one at 1650–1700 cm^{-1} (Fig. 2b). Interestingly, the peaks associated with carbonyls appear at wavenumbers lower than those expected in conventional polyurethanes. It could be argued that they may be related to the stretching vibrations of urea derived carbonyls [18], since forming urea groups during aminolysis of cyclic carbonates in a presence of TBD catalyst was reported before in the literature [24–26]. However, such reactions occur at temperatures significantly higher than those in the current study [24–26], and no other bands associated with urea are present in the spectra at hand, i.e. there are no traces of the bands corresponding to bending vibrations of urea-derived N–H at 1550 cm^{-1} [18,19].

A shift of the bands associated with carbonyls of the same origin towards lower wavenumbers is mainly attributed to hydrogen bonding and is a well-known phenomenon for polyurethanes, including NIPUs [27]. Usually this shift is in the range of 20–30 cm^{-1} and differs based on the number of interacting groups, their ordering state, and general chemical composition of polymer [28]. Here, the shift is closer to 50 cm^{-1}. Such strong shifts of bands towards lower wavenumbers due to hydrogen bonding are not common, however, they have been reported in the literature for carbonyl region in polyurethanes [19,29,30] and poly(hydroxy urethanes) [19,27,31,32]. Strongly shifted bands are associated with the presence of sterically hindered hydrogen-bonded carbonyls [31], and hydrogen bonded carbonyls in ordered state [29,30,32]. This will be further discussed later in the text.

The region associated with stretching vibrations of urethane carbonyls (1600–1750 cm^{-1}) seems to consist of three strongly overlapping components roughly centered around 1720 cm^{-1}, 1700 cm^{-1}, and 1650 cm^{-1} (see also Fig. 3a). Plurality of components in this region is routinely observed in polyurethanes [33] as well as in e.g. polyamides [34]. The highest wavenumber component is generally attributed to "free", i.e. non-hydrogen bonded carbonyls. Upon formation of hydrogen bonds, carbonyl bands shift to lower frequency, and thus the components at lower wavenumbers are attributable to hydrogen bonded carbonyls. The existence of more than one such component is associated with different local conformations [34]. This is most commonly described in terms of "disordered" or "ordered" carbonyls, the latter referring to crystalline domains. Here, however, crystallinity is not observed. The multitude should be sought elsewhere. One possibility is that each peak is related with a carbonyl bonded with a different proton donor. In this case, the less shifted component should be related to carbonyls hydrogen bonded with NH groups while the more shifted ones with the more electronegative OH groups [35]. This hypothesis, however, is not supported by the data - with increasing secondary amines in the system it is the more shifted band that increases in relative intensity. A second possibility is related to the ability of carbonyls to form multiple hydrogen bonds [36]. Double hydrogen bonds are characterized by increased strength and directionality in comparison to single HBs [37]. Therefore, the less shifted component might be associated with carbonyls linked to one donor, and the more shifted one to more coordinated carbonyls linked to two donors [35]. Thus, in the following, we will refer to the 1700 cm^{-1} band as "single H-bonded" and to the 1650 cm^{-1} one as "double H-bonded".

In order to quantify the influence of TETA content, pseudo-Voigt functions in the form of Gaussian-Lorentzian sums were fitted to the components of the carbonyl region (Fig. 3a):

$$y = 2A\left[\frac{s\sqrt{\ln 2}}{w\sqrt{\pi}}\exp\left(-4\ln 2\left(\frac{x-x_c}{w}\right)^2\right)+\frac{1-s}{\pi w\left[1+4\left(\frac{x-x_c}{w}\right)^2\right]}\right] \quad (1)$$

In this equation A is the integral intensity, w is the width of the band, x_c is the center of the band, s is the contribution of the Gaussian term to the sum, i.e. $s = 1$ corresponds to a fully gaussian distribution, while $s = 0$ to a fully lorentzian one.

Except for the three components in the urethane carbonyl region, one similar term was added to account for the band associated with cyclic carbonate carbonyl around 1800 cm^{-1} and one more to account for the contribution of lower wavelength bands (background). Three more small peaks, hardly visible in the scale of Fig. 3a, were added to account for small effects of unknown origin roughly around 1650 and 1820 cm^{-1}.

The strength of the bands is presented in terms of the intensity fraction, i.e. the value of the area of each peak normalized to the sum of the areas of all the peaks associated with polyurethane related carbonyls. Excluding the material without TETA, the relative area (A) (Fig. 3b) of the band correlated with double H-bonded carbonyls shows an increasing trend at the expense of single H-bonded carbonyls. The change is significant, with the relative area of the band correlated to double hydrogen bonded carbonyls being three times higher for T100 material in comparison to T20. Simultaneously, only a minor decreasing trend is observed for the ratio of the component associated with free carbonyls. Evidently, the increase of TETA content mainly influences the nature of already hydrogen-bonded carbonyls, promoting formation of double hydrogen bonds, rather than causing formation of new hydrogen bonds between residual free carbonyls and other moieties. This may indicate that non-hydrogen bonded carbonyls do not originate from lack of moieties able to form hydrogen bonds, but rather from steric hindrances, which are not affected by further introduction of donors or acceptors of HBs.

It is not clear at this point why the material without TETA deviates from the trend. The reason should probably be sought in the higher

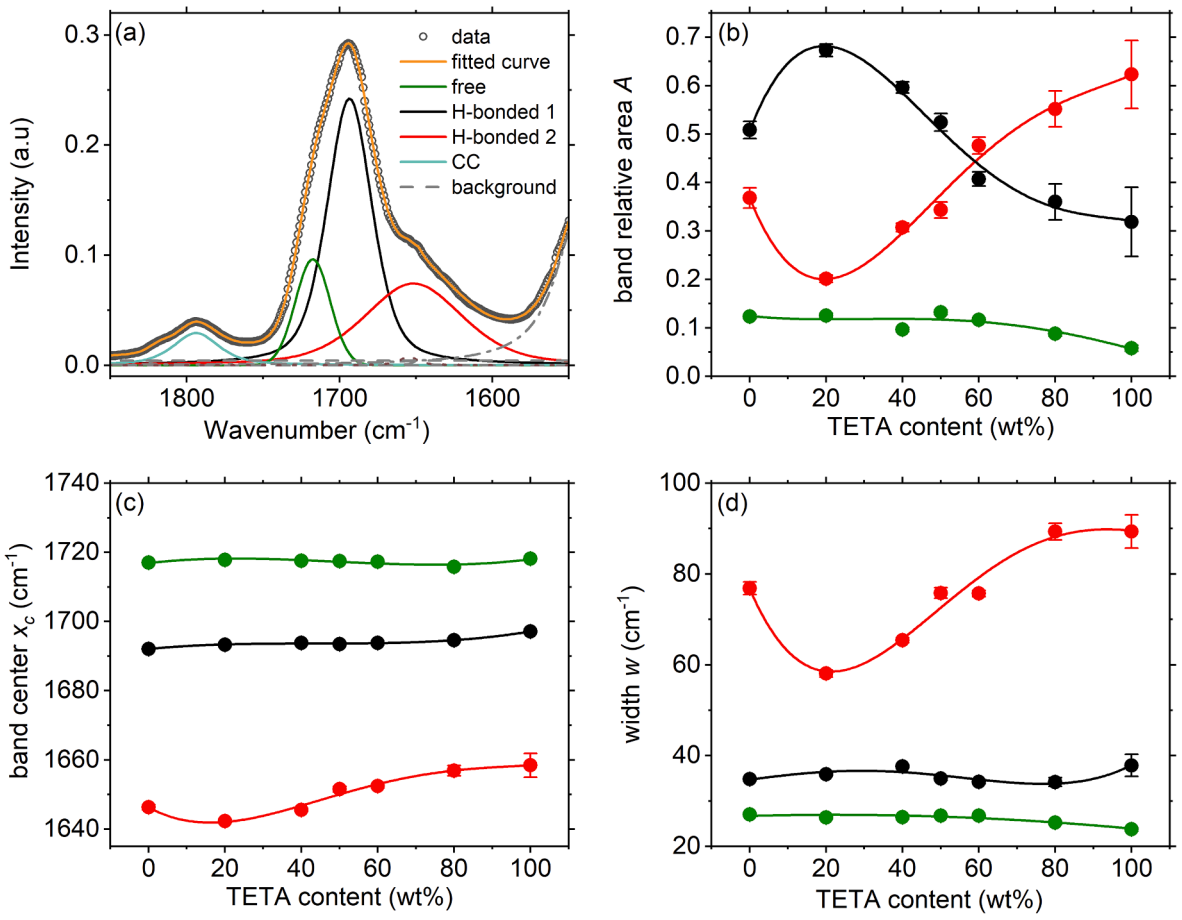

Fig. 3. Fitting of pseudo-Voigt functions to the carbonyls region of FTIR spectra: (a) component bands: 1720 cm^{-1} – free carbonyls, 1700 cm^{-1} – single H-bonded carbonyls (H-bonded 1), 1650 cm^{-1} – double H-bonded carbonyls (H-bonded 2); fitted curve (orange), and raw data (black open circles) for T50 as an example, grey dashed lines correspond to terms considered as a background; (b)-(d) dependence of characteristic parameters of NIPU carbonyl component bands on TETA content. Colours correspond to those of the legend in panel (a). Lines are guides to the eye. (For interpretation of the references to colour in this figure legend, the reader is referred to the web version of this article.)

order along the chain, due to the single amine component. This order likely facilitates the development of more ordered hydrogen networking. It is also worth mentioning that the material with the lowest fraction of double bonded carbonyls is also the only one which is a viscous liquid, unable to form films. Therefore, we attribute the dimensional stability of these materials to those double hydrogen bonds.

The center of component band (x_c) (Fig. 3c) associated with double hydrogen-bonded carbonyls shifts slightly towards higher wavenumbers with increasing TETA content, while the location of component bands associated with free carbonyls and single H-bonded carbonyls seems to be unaffected by material composition. Similar behavior was reported earlier by Queiroz *et al.* for ordered H-bonded carbonyls [38]. The shift of the band of double hydrogen-bonded carbonyls towards higher frequencies implies that the strength of the hydrogen bonds becomes weaker with increasing TETA content [38,39]. The above may originate from the fact that introducing secondary amine groups may disrupt hydrogen bonds formed between urethane-derived carbonyls and –OH groups (inter- and intramolecular) and promote formation of HBs between secondary amino groups and carbonyls, that are weaker than OH-carbonyl ones, since nitrogen is less electronegative in comparison to oxygen [40]. Shifting of the band associated with double hydrogen–bonded carbonyls towards higher wavenumbers upon exchanging one of the donors for a donor with less electronegative atom was reported before by Feldblum and Arkin [35].

Width (w) of the components (Fig. 3d) associated with free carbonyls and single H-bonded carbonyls do not differ significantly between materials with different TETA content. However, the component band of double H-bonded carbonyls broadens significantly with increasing TETA content (up to the width of 90 cm^{-1}). The frequency (and width) of a vibration results from a competition between its attractive (red shifting) and repulsive (blue shifting) components. Changes in the environment will shift vibrational peaks towards blue or red depending on which component is favored [41]. The broadening of double H-bonded carbonyl band might originate from the fact that hydrogen bonds act as discharge paths for the vibrational energy causing the carbonyl vibration to relax rapidly – the faster the relaxation (the shorter lifetime), the broader is the band [41]. The band broadens because of the rapid energy relaxation caused by the hydrogen bonds between secondary amino groups originating from TETA and urethane-derived carbonyls.

3.2. *Glass transition – DSC*

In DSC curves the only visible event is the glass transition step (Figure S5 in Supplementary Material). Fig. 4a shows the dependence of glass transition temperature on TETA content along with the corresponding onset and end points. Introduction of 20 wt% TETA to the amine reagent results in a significant drop in T_g, while increasing TETA content up to 80 wt%, results in increasing glass transition temperature, which stays in agreement with the dependency of double H-bonded carbonyls density on TETA content reported in section 3.1.1 and the fact that intermolecular hydrogen bonds hinder mobility of polymer chains [42,43]. The most significant change occurs between materials T60 and

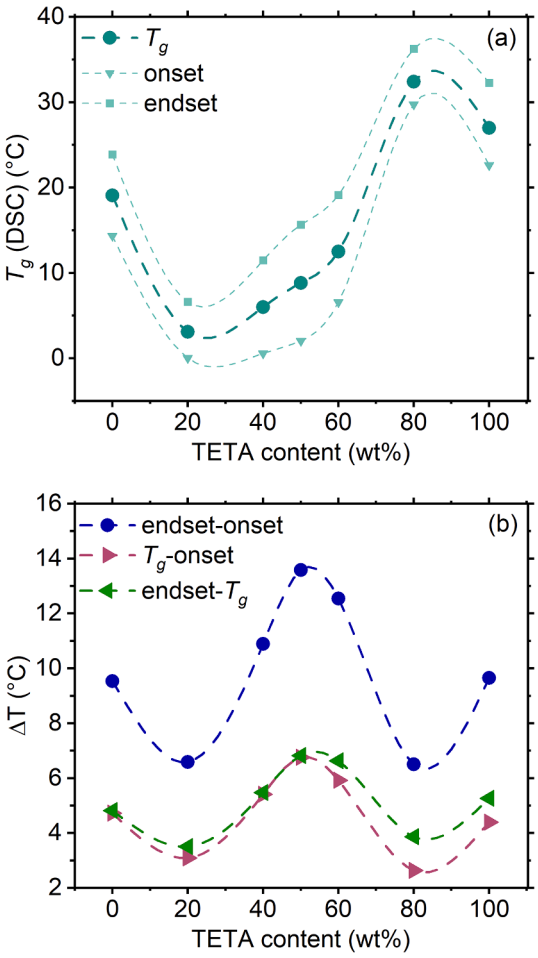

Fig. 4. (a) Glass transition temperature as a function of TETA content. Smaller symbols indicate the onset and end of the transition, (b) width of glass transition step and distance of onset and end point from the midpoint, for the evaluation of asymmetry.

T80, with T80 exhibiting the highest glass transition temperature among all studied materials. It is noteworthy that despite further increase of TETA content to 100 wt%, the glass temperature notably decreases. This deviation might be associated with the formation of HB-rich and HB-deficient regions - with majority of carbonyls forming two hydrogen bonds each, formation of H–bond rich regions might be promoted, in a similar fashion to traditional segmented polyurethanes allowing the formation of polyether-rich regions with increased mobility [44,45].

The width of the glass transition in the temperature range can be considered as a measure of inhomogeneity of the system [46]. Here, the widest glass transition occurs around 50 wt% TETA content (Fig. 4b), which indicates lowest degree of homogeneity of these materials [46]. Interestingly, the narrowest glass transition is observed for materials containing 20 wt% and 80 wt% TETA, which may seem contradictory since both of those materials were synthesized using two types of amines, and thus should exhibit lower homogeneity than materials based on only one amine reagent. Therefore, it may be concluded that introducing small amount of second amine reagent allows for better homogeneity of NIPU materials, while the pure components seem to create higher heterogeneity. In order to study the asymmetry of the step, we compare the distances between the midpoint and the extrema of the step, i.e. the onset and end temperatures. It may be observed that for samples up to T50, glass transition is symmetric. However, with increasing TETA content it becomes more asymmetric with broadening on the high temperature side. We will come back to this point later when studying the glass transition with DMA and BDS.

For completeness, we would like to mention that the values of Δc_P show variation within the experimental inaccuracy, and are in the range 0.58–0.64 J/gK.

3.3. *Mechanical properties – Dynamic mechanical analysis*

Materials in the range 50–100 wt% TETA were studied by DMA, while the rest of them lacked the required structural integrity. More prominently, the sample with 20 wt% TETA is a viscous liquid. In fact, samples with 50 and 60 wt% TETA also broke during the experiment at slightly elevated temperatures. The storage modulus (E') and tanδ as a function of temperature are shown in Fig. 5.

As expected, the mechanical modulus shows a decreasing trend with temperature, forming a step corresponding to the glass transition in the region 0–80 °C (Fig. 5a, Table 1). In general, materials with high TETA content exhibit relatively high glassy modulus (1500–4000 MPa), especially in comparison with other NIPUs, and especially linear ones [47–52]. Materials with higher TETA content exhibit higher storage modulus both in the glassy and rubbery region. This should be attributed to the denser hydrogen bonding already observed by FTIR [53–55] (Table 1).

An interesting observation is that mechanical properties correlate well with the density of hydrogen bonds, even for the materials where mechanical moduli were not possible to measure (Fig. 3b, Table 1). Material T20 exhibits the lowest density of double H–bonded carbonyls and is a viscous liquid. T0 and T40 with slightly higher double hydrogen bond density, are solids, but too soft to be measured. Then, materials from T50 to T100 show progressively higher double hydrogen bond density, as well as increasing mechanical moduli. Thus, modulating density of hydrogen bonding through introduction of HB donors proves to be useful method for tailoring NIPUs mechanical properties.

The maximum at tanδ curve ($T_{\alpha,5Hz}$) (Fig. 5b) may be used as a measure of the glass transition temperature [56–59]. Indeed, in the studied TETA content range its trends are in agreement with those of the calorimetric T_g. The loss tangent peaks shift to higher temperatures is usually associated with higher crosslink density [60]. NIPUs under investigation exhibit relatively broad transition region (Fig. 5b) of about 40–60 °C, depending on TETA content. Interestingly, increasing TETA content up to 80 wt% gives a rise to a shoulder at lower temperatures side. This smaller peak is more separated by the main one for the high TETA content materials. A plausible hypothesis is that it is related to faster dynamics in regions with lower hydrogen bonding density. This would however imply the existence of a minor phase separation. We will

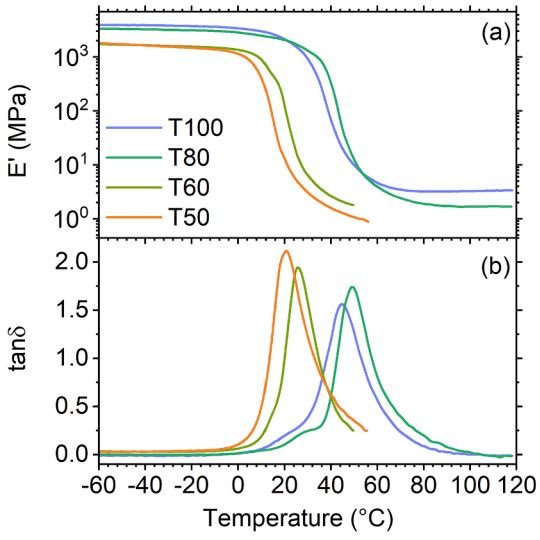

Fig. 5. DMA curves recorded for selected NIPUs at 5 Hz: storage modulus (a) and loss tangent (b) as a function of temperature.

Table 1
Glassy and mechanical moduli of all materials under investigation, or a qualitative comment about their physical state.

Material	Glassy modulus (MPa)	Rubbery modulus (MPa)
T0	Too soft to measure	
T20	Viscous liquid	
T40	Too soft to measure	
T50	1547	Broke before the plateau
T60	1682	Broke before the plateau
T80	3302	1.7
T100	3898	3.2

come back to this point later when co-evaluating the results of all methods regarding glass transition.

All the studied materials exhibit values of loss tangent (tanδ) above 1.5 (Fig. 5b). As the TETA content increases, values of tanδ decrease. This originates from restrictions in energy dissipation in the material due to lower degree of chain motion [61], e.g. due to higher hydrogen bonding. The most noticeable reduction in tanδ value is observed comparing T60 and T80 samples. Interestingly, the differences in tanδ values between T50 and T60 or T80 and T100 are not so pronounced. Yet, the significant decrease in the value of the tanδ takes place when increasing TETA content in amine reagents from 60 wt% to 80 wt%. The origin of the above is yet unclear.

3.4. Molecular mobility – Broadband dielectric spectroscopy

The dielectric spectra of the materials are quite rich in features. We will present the results starting with the α relaxation associated with the dynamic glass transition at temperatures above T_g. Then we will proceed to the local relaxations γ and β appearing at lower temperatures. We will finish with a study of the charge transport, in terms of dc conductivity which is quite strong in the systems at hand.

3.4.1. Dynamic glass transition – α relaxation

The α relaxation is associated with the dynamic glass transition of the system. Its high frequency wing is first visible in the experimental window at around 10 °C and stays in the experimental window up to the maximum temperature of the experiment, i.e. 90 °C (Fig. 6).

The relaxation manifests itself as a broad step in the real part of dielectric function spectra (Fig. 6a), accompanied at the low frequencies side by an upturn corresponding to parasitic electrode polarization. Strong dc-conductivity, visible as a slope in the imaginary part of dielectric function (ε'') spectra (Fig. 6b), masks completely the peak of the α relaxation. Therefore, in order to quantify the characteristics of α relaxation, we followed an approach proposed by Wübbenhorst and van Turnhout [62]. By this approach, the conductivity-free, polarization-related component of ε'' can be approximated by the partial derivative of ε' with the logarithm of frequency:

$$\varepsilon''_{der}(f) = -\frac{\pi}{2}\frac{\partial \varepsilon'(f)}{\partial \ln f} \tag{2}$$

Upon this calculation, the resulting spectra are shown in Fig. 7c. Although still partially masked by electrode polarization, relatively clear peaks are observed. At 50 °C the peaks are the best visible for all materials in the frequency window of the experiments (Fig. 7).

In perfect agreement with the trends of the calorimetric glass transition temperature (Section 3.2, Fig. 4a), starting from the pure DAB material, 20 wt% TETA causes a significant acceleration of dynamics, which is then counteracted gradually with increasing TETA content. At the end, a small acceleration is observed again when moving from the 80 wt% TETA material to the pure TETA one.

The ε''_{der} spectra can be fitted well by a combination of Equation (2) and the well tested Havriliak–Negami model [63–65]:

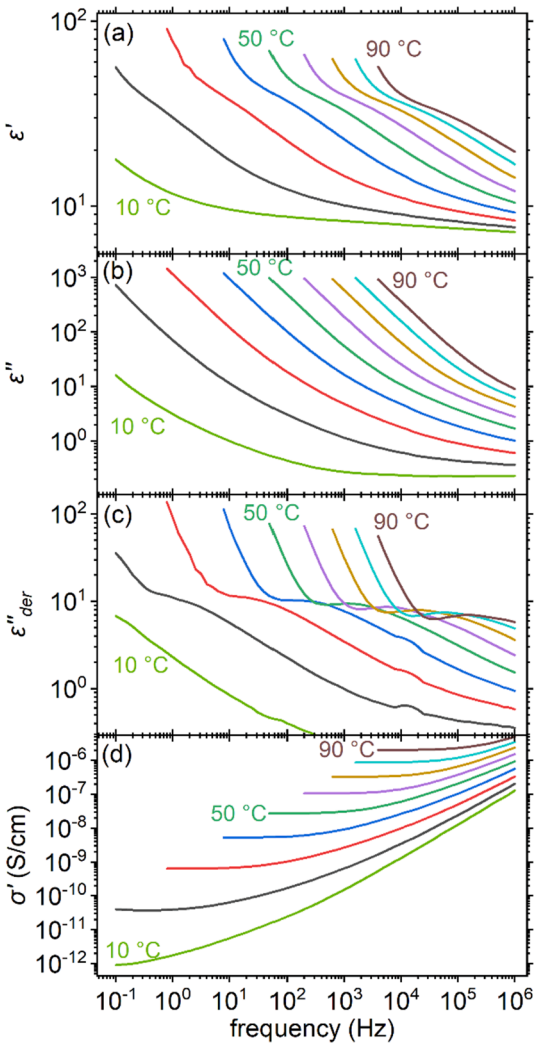

Fig. 6. Various formalisms of dielectric spectra of material T50 in the temperature range where dynamic glass transition is in the frequency window; in steps of 10 K. Key temperatures are annotated. Region dominated by electrode polarization has been omitted. (a) real part of dielectric function, (b) imaginary part of dielectric function, (c) „conductivity-free" ε'' calculated on the basis of Wübbenhorst and van Turnhout's method (details in text), (d) real part of conductivity.

$$\varepsilon^*(f) = \frac{\Delta\varepsilon}{\left(1 + \left(i\frac{f}{f_{HN}}\right)^a\right)^\gamma} \tag{3}$$

along with a power law to account for electrode polarization at low frequencies.

In Equation (3), f_{HN} is a relaxation frequency, $\Delta\varepsilon$ the contribution of the studied polarization mechanism to the static dielectric constant of the material, and a and γ are shape exponents.

The quality of the fit with a single Havriliak-Negami term is remarkable (Fig. 7), contrary to what is usually observed in polyurethanes [45,66] and poly(hydroxy urethanes) [67] or even poly (propylene oxide) [68,69]. This should be related to the lack of inhomogeneities in the nanoscale observed in typical polyurethanes, and to the small molar mass of PPO fragments which prohibits the emergence of a normal mode relaxation.

We will present the results of this analysis, starting with the time scale in terms of the peak frequency f_{max} of the relaxation. It is calculated as a function of the characteristic frequency and the shape exponents as given in Equation (4) [70]:

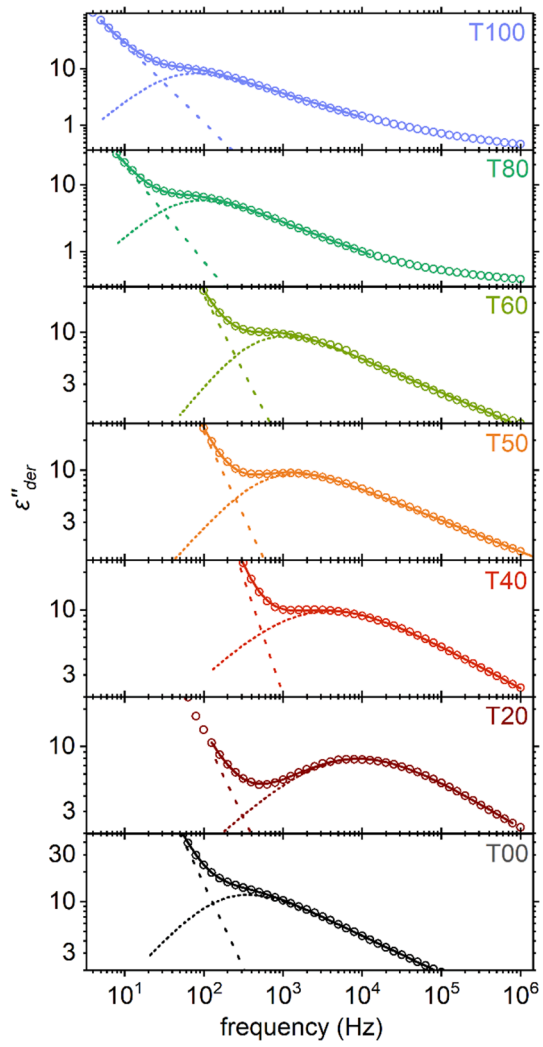

Fig. 7. ε''_{der} spectra calculated for all materials at 50 °C. Continuous lines are fits of a Havriliak-Negami model and a power law. Dotted and dashed lines are the individual components respectively. Details in text.

$$f_{max} = f_{HN}\left(\frac{\sin\left(\frac{a}{1+\gamma}\frac{\pi}{2}\right)}{\sin\left(\frac{a\gamma}{1+\gamma}\frac{\pi}{2}\right)}\right)^{\frac{1}{a}} \tag{4}$$

The traces of α relaxation on the Arrhenius plot lie at temperatures more than 80 K higher than those of pure PPO as reported by various authors (Fig. 8a). This is an interesting observation. The majority component of the systems, with more than 70 wt%, is carbonate derived PPO blocks. Meanwhile, amine components lack side chains or rigid structures, and to a large extent could be regarded as short links, effectively extending oligomeric PPO. Moreover, according to the literature, α relaxation of PPO is largely unaffected by molar mass already starting at $M_w = 400$ g/mol, i.e. entanglements are already the dominant effect in mobility. Therefore, under the assumption of not interacting segments, the α relaxation of our materials should lie very close to that of pure PPO. This is clearly disproven by the experiment. The extreme migration to higher temperatures, corresponding to hindered mobility, should be sought in the hydrogen bonding entities that are in abundance as FTIR has explicitly shown.

We now turn our attention to the dependence of the dynamic glass transition on TETA content (Fig. 8b). As expected, the traces follow a concave trace, which is typical for the dynamic glass transition. The trends are the same as those of the calorimetric glass transition

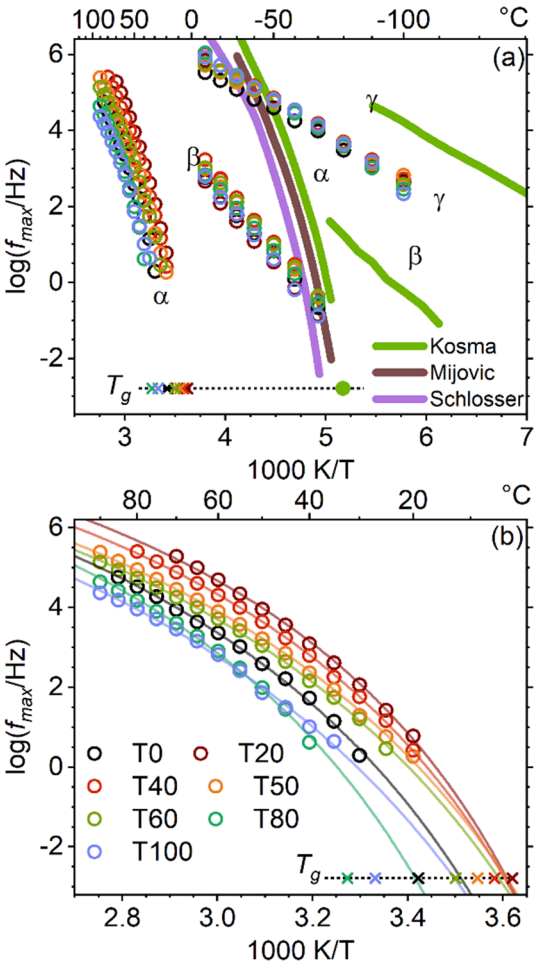

Fig. 8. Arrhenius plots for all materials under investigation. Calorimetric glass transition temperatures are plotted at the frequency corresponding to the equivalent relaxation time of 100 s. A broad perspective including all relaxations in this study is drawn as points in panel (a). For clarity, the legend is shown in panel (b). Lines are traces on which relaxations of PPO with varying molar mass collapse as reported in the literature: Kosma et al.[68] $M_w = 400$ and 2 k, Mijovic et al.[71] $M_w = 2$ k-12 k, Schlosser et al.[69] $M_w = 1$ k-4 k. Normal mode relaxations from the literature have been omitted for clarity. The kind of each relaxation is annotated near the traces. (b) a focus on the α relaxation traces in the current study. Lines are fits of Vogel-Fulcher-Tammann-Hesse (VFTH) equation.

temperature, with the exception of the T80 and T100 materials above 60 °C, where an inversion is observed.

The traces can be described by the empirical Vogel-Fulcher-Tammann-Hesse (VFTH) equation [72–74] in a form proposed by Angel [75]:

$$f_{max} = f_p \cdot e^{-\frac{DT_0}{T-T_0}} \tag{5}$$

In this equation, T_0 is the Vogel temperature, i.e. the temperature below which all cooperative mobility ceases, f_p is the so-called phonon frequency, and D the so-called strength parameter. The smaller the D is, the higher the fragility of the relaxation, i.e. the stronger its cooperative nature [63]. An initial fit showed negligible variation for f_p, so in order to enhance statistical significance of the rest of the parameters, we performed a simultaneous fit of the traces with a common f_p. The fitting procedure yielded $f_p = 10^{11.06\pm0.20}$ Hz which is a reasonable value, in the range expected for polymers [63]. T_0 doesn't show strong trends with TETA content (Fig. 9a). D (Fig. 9b) on the other hand, seems to drop significantly between the pure DAB material and the 20 wt% TETA one, and then rise quite monotonically up to TETA content 100 wt%. That is,

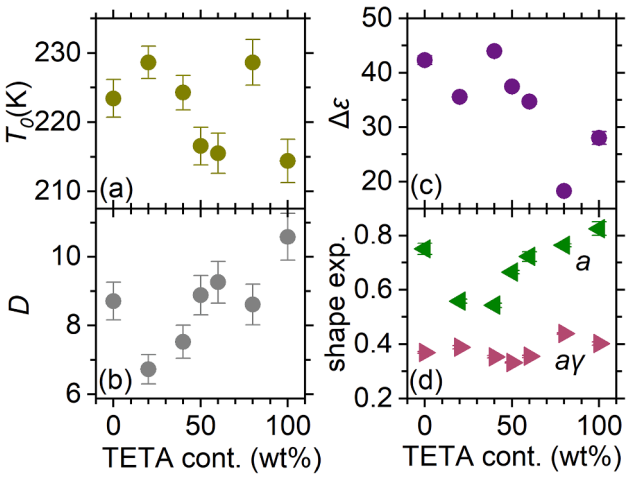

Fig. 9. Selected parameters of α relaxation as a function of TETA content. (a) Vogel temperature, (b) strength parameter, (c) relaxation strength at 50 °C, (d) shape parameters at 50 °C. Details in text.

we may assume maximum cooperativity of the relaxation around 20 wt % TETA content. This dependence resembles the dependence of relative density of double- and single hydrogen-bonded carbonyls in FTIR spectra (Fig. 3b). There seems to be a negative correlation between the fraction of double hydrogen bonded carbonyls and the cooperativity of the system. This is compatible with a decrease of fragility observed with increasing crosslinking density in an epoxy resin system [76].

Regarding the strength $\Delta\varepsilon$, and shape exponents of the relaxation, we will show results obtained at 50 °C, i.e. a temperature where the α relaxation of all materials was close to the center of the frequency window.

Despite some scattering, $\Delta\varepsilon$ shows a decreasing trend with TETA content (Fig. 9c). At a first glance, this is somewhat unexpected. On one hand, Δc_P showed relative stability (section 3.2) with TETA content, so overall mobility does not seem to be restricted. Moreover, more polar groups are introduced in the system, which would be expected to provide better overall polarizability. However, this is not the case. Instead, the polarizability originating from segmental motion of chains seems to be restricted. This could again be related to the increase of hydrogen bonding density, which would restrict polarizability of the more polar groups, without affecting radically the non-polar ones.

Havriliak-Negami model on the low frequency side behaves like $\varepsilon'' \propto f^{a}$ whereas on the high frequency side as $\varepsilon'' \propto f^{-a\gamma}$ [63]. Hence parameters a and $a\gamma$ denote the low and high frequency slopes of the relaxation, respectively. Smaller a and $a\gamma$ denote a broader relaxation, i.e. a broader distribution of relaxation times. On the other hand, the high frequency side corresponds to „faster" dipoles, and the low frequency one to „slower" dipoles. In that respect, Fig. 9d shows that TETA has negligible effect on the distribution of fast dipoles. On the contrary, there seems to be a quite strong dependence on the distribution of slow dipoles, which correspond to longer range mobility. The distribution seems to be more heterogeneous in a region around 20–40 wt% TETA. This again resembles the relative density of double hydrogen bonds (Fig. 3b) as well as the width of the relevant peak (Fig. 3d) in FTIR spectra. This correlation may be understood by the intuitive assumption that "slower" segments should be expected around hydrogen bonded sites. A higher heterogeneity of the strength of these bonds should be translated to the heterogeneity in mobility.

3.4.2. Local mobility - β, γ relaxations

At temperatures below 0 °C, two secondary relaxations appear in the ε'' curves (Figure S6 in Supplementary Material). The one at higher frequencies is the γ relaxation, which in conventional polyurethanes is typically attributed to crankshaft motions along the chain contour of the polyether component. The slower one, β relaxation, in conventional polyurethanes is attributed to fluctuations of the carbonyl unit of the urethane bond with attached water molecules [77]. Indeed, in conventional polyurethanes, it has been shown to disappear upon careful drying [77]. Here, this is not the case: a well-defined strong peak is present. A difference from conventional polyurethanes is the hydroxyl accompanying the urethane bond, and at this point we tentatively attribute the relaxation to this group.

Cole-Cole model functions, i.e. Havriliak-Negami (Equation (3) with $\gamma = 1$, were fitted to the spectra, as is typical for local relaxations [63].

Here we will focus on the dynamics of the relaxations in terms of their characteristic frequency (Figure S6 in Supplementary Material). The other, less significant parameters are reported to some extent in the Supplementary Material (Figure S7). Although it originates from the bulk of the polyether, γ relaxation is somewhat slower than in PPO. A similar phenomenon was observed when PPO of similar molar mass was confined in an epoxy network [68]. The effect in that system should be attributed to the most compact arrangements of chains and the thus enhanced inter- and intra-chain interactions. Interestingly, however, here we have no covalent bonds that could make the structure more compact. This role should be assigned to hydrogen bonding between neighboring segments.

A fit of the Arrhenius model to the data yields activation energies in the range 0.28–0.36 eV (Fig. S7c in Supplementary Material), which is in agreement with the value for pure PPO diamine, reported by Kosma *et al.* [68] as 0.306 ± 0.003 eV. Despite some scattering, a weak increasing trend of the activation energy is visible with increasing TETA content, indicating a very weak hindering effect on the γ relaxation in the materials at hand. This should be likely associated with hydrogen bonding between secondary amine groups and ether groups along the polyether contour.

The traces of β relaxation in the Arrhenius plot are more spread out than those of γ relaxation; however, there is no significant variation of the activation energy with TETA content and its values are around 0.6 eV, which is significantly higher than that of the β relaxation of PPO (0.48 ± 0.01 eV) [68], which indicates that the two relaxations are of quite different origin.

3.4.3. Conductivity

DC conductivity σ_{dc} was measured at the low frequency plateau on the spectra of the real part of conductivity $\sigma'(f)$ (Fig. 6d). The values are presented as a function of temperature in the Arrhenius plot of Fig. 10a.

The dependence of σ_{dc} with temperature is a concave one, indicating a collaborative conduction mechanism. Interestingly, the observed trends with TETA resemble very much those observed for the time scale of α relaxation, which is a hint that conductivity is coupled with the dynamic glass transition. In order to further follow this point, we plotted the values of conductivity against those of the peak frequency f_{max} of the α relaxation (Fig. 10b). Indeed, the hypothesis is confirmed, as traces of all samples do not deviate much from each other. The more pronounced deviation is observed for the high TETA content materials for which an additional component of α relaxation has been observed by DMA.

3.5. The effect of TETA on glass transition

Before we conclude, we would like to compare results regarding glass transition obtained by three different methods, and make some comments that are of interest from the methodological point of view.

In order to compare results from BDS to those of the other techniques, the fitted VFT curves were extrapolated to the frequency corresponding to relaxation time $\tau = 100$s. Thus, the so-called dielectric glass transition temperature $T_{g,diel}$, a third measure of the glass transition temperature is defined. This value, along with the calorimetric T_g and the peak temperature of the α relaxation as recorded with DMA at frequency 5 Hz ($T_{a,5Hz}$) are plotted as a function of TETA content in Fig. 11.

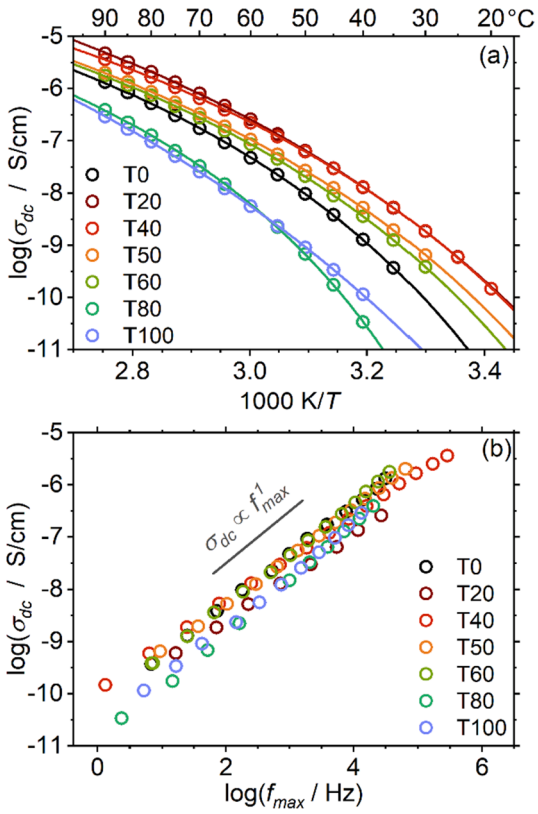

Fig. 10. (a) Arrhenius plot of dc conductivity for all materials under investigation. Lines are fits of a VFTH function. (b) The same values plotted against the frequency of the maximum of the α relaxation at the same temperature (data from Fig. 8).

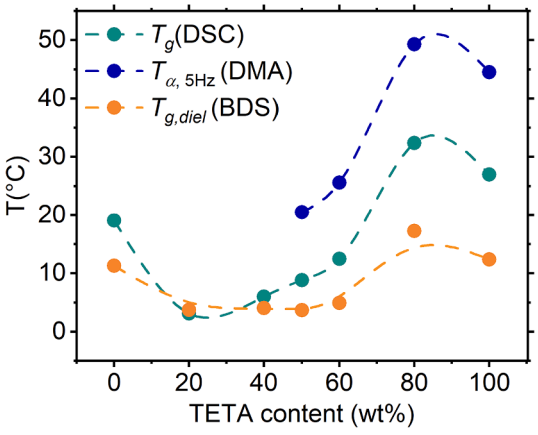

Fig. 11. Glass transition temperatures as a function of TETA content obtained by different methods.

Although the value of T_g differs depending on the methods used for its analysis, trends observed by the three methods are in agreement with each other. It is clear that increased TETA content and subsequently higher density of doubly hydrogen bonded carbonyls correlates with reduced mobility. Interestingly, the material without TETA also shows a higher density of doubly bonded carbonyls and a slower mobility than its neighboring sample with 20 wt% TETA.

Surprisingly, DMA curves showed a component faster than the main glass transition event, which is more clearly visible at high TETA content (80–100 wt%). This component was not visible in the other two methods, however it may be manifested as an increase in asymmetry of DSC steps and as a change of slope in the high temperature side of the α relaxation in dielectric spectra. The reason should be sought in potential differences between the responses of this component to different stimuli, i.e. this component is more sensitive to mechanical stimulus than to thermal and dielectric ones.

With respect to the strength of the glass transition event, there is an apparent disagreement between DSC and dielectric spectroscopy. While Δc_P does not show a significant dependence on TETA content, the $\Delta\varepsilon$ values decrease considerably. This should be also attributed to the interplay between dielectric and thermal responses of hydrogen bonded and "free" chain segments.

4. Conclusions

A series of NIPU with different TETA:DAB ratios was synthesized in order to study the effects of secondary amino groups on the hydrogen bonding and, subsequently, on the molecular dynamics and mechanical properties. Despite amine reagent consisting only about ~ 20 % of the polymer mass, it was shown that introducing amine component bearing secondary amino groups, which act as hydrogen bond donors, strongly influences NIPUs properties. Thus, it possible to tailor chain mobility and mechanical properties of NIPUs by modulating hydrogen bonding density.

FTIR analysis showed a splitting of the urethane carbonyl band into three components attributable to free, single H-bonded, and double H-bonded carbonyls. The secondary amino groups on TETA chain act as hydrogen bond donors, however, they do not influence significantly the density of "free" carbonyls. Instead, they form additional hydrogen bonds on already bonded carbonyls. The material based on DAB deviates from the trend, which may be attributed to increased chain packing due to stricter periodicity of the chain.

Differential scanning calorimetry, dynamic mechanical analysis and broadband dielectric spectroscopy, in agreement with each other, show that molecular mobility of poly(hydroxy urethanes) is significantly slowed down (migrated to higher temperatures) as compared to that of PPO. This is interesting, because PPO-based cyclic carbonate accounts for around 80 % of the materials mass. The effect should be attributed to restrictions in mobility due to hydrogen bonding. Indeed, for materials containing up to 80 % TETA in the mass of amine reagents, higher T_g correlates with higher contribution of the FTIR component related to double H-bonded carbonyls. The material based solely on TETA deviates from this trend.

At higher TETA content materials, a second component appears at DMA tanδ curves at the low temperature side of the main α relaxation (dynamic glass transition). This low temperature relaxation seems to respond only to mechanical stimulus, while it has very weak - if any - thermal and dielectric response. These observations are compatible with a phase-separated morphology, the nature of which needs to be studied in a future work. Dielectric spectroscopy showed correlation between higher density of double H-bonded carbonyls and lower cooperativity of segmental dynamics (dynamic glass transition). It also showed a very strong coupling of charge and segmental mobility.

The density of double-bound carbonyls correlates strongly with the mechanical properties and is a key factor determining state, shape stability, and mechanical strength of the studied NIPUs. The sample with the lowest content of additional HB donor groups (T20) is a viscous liquid, intermediate content result in materials which form soft and brittle films, while higher content of HB donors, and thus higher density of hydrogen bonding, results in mechanically stable, durable elastomers. The storage modulus of those elastomers correlates positively with the contribution of double-bound carbonyls in the FTIR spectra, and is increase almost threefold by increasing TETA content in amine reagents from 50 wt% to 100 wt%. The studied NIPUs exhibit relatively high values of tanδ (over 1.5), rendering them interesting from the point of view of technological applications (e.g. good vibration damping). Changing the TETA content allows for tailoring the temperature region

at which materials exhibit high tanδ values.

Future study should focus on explaining the origins of the small component observed for α relaxation in the high TETA content materials by DMA, as well as on the peculiar behavior at low TETA contents i.e. uncovering the reason behind inhibition of hydrogen bonding upon small addition of secondary amino groups. It is also known that poly (hydroxy urethanes) are highly hydrophilic [67], and therefore it would be valuable to study how water affects hydrogen bonding density and nature of hydrogen bonded carbonyls.

CRediT authorship contribution statement

Izabela Łukaszewska: Conceptualization, Methodology, Formal analysis, Investigation, Data curation, Writing – original draft, Visualization. **Sebastian Lalik:** Investigation, Writing – review & editing, Methodology, Investigation, Writing – review & editing. **Artur Bukowczan:** Methodology, Investigation, Writing – review & editing. **Monika Marzec:** Resources, Writing – review & editing, Supervision, Funding acquisition. **Krzysztof Pielichowski:** Resources, Writing – review & editing, Supervision, Funding acquisition. **Konstantinos N. Raftopoulos:** Conceptualization, Formal analysis, Data curation, Writing – original draft, Visualization, Supervision.

Declaration of Competing Interest

The authors declare that they have no known competing financial interests or personal relationships that could have appeared to influence the work reported in this paper.

Data availability

Data will be made available on request.

Acknowledgements

This research was funded by the National Research Center in Poland (Narodowe Centrum Nauki, NCN), under contract number 2017/27/B/ST8/01584.

The research was carried out with equipment purchased thanks to the financial support of the European Regional Development Fund in the framework of the Polish Innovation Economy Operational Program, Contract No. POIG.02.01.00–12–023/08 (Novocontrol spectrometer).

This research was supported in part by the Excellence Initiative – Research University Program at the Jagiellonian University in Kraków.

Data analysis was carried out with software *Grafity*, created and freely distributed (grafitylabs.com) by Dr. Daniel Fragiadakis, to whom we express our gratitude.

Appendix A. Supplementary material

Supplementary data to this article can be found online at https://doi.org/10.1016/j.molliq.2023.123263.

References

[1] A. Das, P. Mahanwar, A brief discussion on advances in polyurethane applications, Adv. Ind. Eng. Polym. Res. 3 (2020) 93–101, https://doi.org/10.1016/J.AIEPR.2020.07.002.

[2] A. Cornille, R. Auvergne, O. Figovsky, B. Boutevin, S. Caillol, A perspective approach to sustainable routes for non-isocyanate polyurethanes, Eur. Polym. J. 87 (2017) 535–552, https://doi.org/10.1016/j.eurpolymj.2016.11.027.

[3] G. Rokicki, P.G. Parzuchowski, M. Mazurek, Non-isocyanate polyurethanes: synthesis, properties, and applications, Polym. Adv. Technol. 26 (2015) 707–761, https://doi.org/10.1002/pat.3522.

[4] A. Farhadian, A. Ahmadi, I. Omrani, A.B. Miyardan, M.A. Varfolomeev, M. R. Nabid, Synthesis of fully bio-based and solvent free non-isocyanate poly (ester amide/urethane) networks with improved thermal stability on the basis of vegetable oils, Polym. Degrad. Stab. 155 (2018) 111–121, https://doi.org/10.1016/J.POLYMDEGRADSTAB.2018.07.010.

[5] Z. Shen, L. Zheng, C. Li, G. Liu, Y. Xiao, S. Wu, J. Liu, B. Zhang, A comparison of non-isocyanate and HDI-based poly(ether urethane): structure and properties, Polymer (guildf). 175 (2019) 186–194, https://doi.org/10.1016/j.polymer.2019.05.010.

[6] M. Bähr, A. Bitto, R. Mülhaupt, Cyclic limonene dicarbonate as a new monomer for non-isocyanate oligo- and polyurethanes (NIPU) based upon terpenes, Green Chem. 14 (2012) 1447–1454, https://doi.org/10.1039/c2gc35099h.

[7] T. Wang, H. Deng, N. Li, F. Xie, H. Shi, M. Wu, C. Zhang, Mechanically strong non-isocyanate polyurethane thermosets from cyclic carbonate linseed oil, Green Chem. 24 (2022) 8355–8366, https://doi.org/10.1039/D2GC02910C.

[8] M. Bourguignon, J.M. Thomassin, B. Grignard, C. Jerome, C. Detrembleur, Fast and facile one-pot one-step preparation of nonisocyanate polyurethane hydrogels in water at room temperature, ACS Sustain. Chem. Eng. 7 (2019) 12601–12610, https://doi.org/10.1021/acssuschemeng.9b02624.

[9] M. Bourguignon, J.M. Thomassin, B. Grignard, B. Vertruyen, C. Detrembleur, Water-borne isocyanate-free polyurethane hydrogels with adaptable functionality and behavior, Macromol. Rapid Commun. 42 (2021), https://doi.org/10.1002/marc.202000482.

[10] S. Samanta, S. Selvakumar, J. Bahr, D.S. Wickramaratne, M. Sibi, B.J. Chisholm, Synthesis and characterization of polyurethane networks derived from soybean-oil-based cyclic carbonates and bioderivable diamines, ACS Sustain. Chem. Eng. 4 (2016) 6551–6561, https://doi.org/10.1021/acssuschemeng.6b01409.

[11] L. Zhang, X. Luo, Y. Qin, Y. Li, A novel 2,5-furandicarboxylic acid-based bis(cyclic carbonate) for the synthesis of biobased non-isocyanate polyurethanes, RSC Adv. 7 (2016) 37–46, https://doi.org/10.1039/C6RA25045A.

[12] S. Doley, S.K. Dolui, Solvent and catalyst-free synthesis of sunflower oil based polyurethane through non-isocyanate route and its coatings properties, Eur. Polym. J. 102 (2018) 161–168, https://doi.org/10.1016/J.EURPOLYMJ.2018.03.030.

[13] X. Huang, S. Nakagawa, H. Houjou, N. Yoshie, Insights into the role of hydrogen bonds on the mechanical properties of polymer networks, Macromolecules. 54 (2021) 4070–4080, https://doi.org/10.1021/ACS.MACROMOL.1C00120/ASSET/IMAGES/LARGE/MA1C00120_0008.JPEG.

[14] E.D. Głowacki, M. Irimia-Vladu, S. Bauer, N.S. Sariciftci, Hydrogen-bonds in molecular solids-from biological systems to organic electronics, J. Mater. Chem. b. 1 (2013) 3742–3753, https://doi.org/10.1039/C3TB20193G.

[15] H. Yu, Q. Xiao, G. Qi, F. Chen, B. Tu, S. Zhang, Y. Li, Y. Chen, H. Yu, P. Duan, A hydrogen bonds-crosslinked hydrogels with self-healing and adhesive properties for hemostatic, Front. Bioeng. Biotechnol. 10 (2022) 537, https://doi.org/10.3389/FBIOE.2022.855013/BIBTEX.

[16] M.A.C.M. Haniffa, Y.C. Ching, C.H. Chuah, Y.C. Kuan, D.S. Liu, N.S. Liou, Synthesis, characterization and the solvent effects on interfacial phenomena of jatropha curcas oil based non-isocyanate polyurethane, Polymers (basel). 9 (2017), https://doi.org/10.3390/polym9050162.

[17] Z. Wu, W. Cai, R. Chen, J. Qu, Synthesis and properties of ambient-curable non-isocyanate polyurethanes, Prog. Org. Coatings. 119 (2018) 116–122, https://doi.org/10.1016/j.porgcoat.2018.02.006.

[18] M. Buchaca, F. De La Cruz-Martínez, E. Francés-Poveda, J. Fernández-Baeza, L.F. Sánchez-Barba, A. Garcés, J.A. Castro-Osma, A. Lara-Sánchez, M. Martínez De Sarasa Buchaca, F. De La Cruz-Martínez, E. Francés-Poveda, J. Fernández-Baeza, L. F. Sánchez-Barba, A. Garcés, J.A. Castro-Osma, A. Lara-Sánchez, Synthesis of Nonisocyanate Poly(hydroxy)urethanes from Bis(cyclic carbonates) and Polyamines, Polym. 2022, Vol. 14, Page 2719. 14 (2022) 2719. https://doi.org/10.3390/POLYM14132719.

[19] K. Błażek, H. Beneš, Z. Walterová, S. Abbrent, A. Eceiza, T. Calvo-Correas, J. Datta, Synthesis and structural characterization of bio-based bis(cyclic carbonate)s for the preparation of non-isocyanate polyurethanes, Polym. Chem. 12 (2021) 1643–1652, https://doi.org/10.1039/D0PY01576H.

[20] C. Liu, J. Wu, X. Zhou, X. Zhou, Z. Wu, J. Qu, Synthesis and properties of poly (dimethylsiloxane)-based non-isocyanate polyurethanes coatings with good anti-smudge properties, Prog. Org. Coatings. 163 (2022), 106690, https://doi.org/10.1016/j.porgcoat.2021.106690.

[21] P. Saha, L. Goswami, B.S. Kim, Novel biobased non-isocyanate polyurethanes from microbially produced 7,10-dihydroxy-8(E)-octadecenoic acid for potential packaging and coating applications, ACS Sustain. Chem. Eng. 10 (2022) 4623–4633, https://doi.org/10.1021/acssuschemeng.1c08718.

[22] Y. Wang, Y.Y. Ma, W.L. Mo, W.T. Gong, F.Y. Ma, X.Y. Wei, X. Fan, S.P. Zhang, Functional groups of sequential extracts and corresponding residues from Hefeng sub-bituminous coal based on FT-IR analysis, J. Fuel Chem. Technol. 49 (2021) 890–901, https://doi.org/10.1016/S1872-5813(21)60055-5.

[23] X. Zhang, F. Lin, Q. Yuan, L. Zhu, C. Wang, S. Yang, Hydrogen-bonded thin films of cellulose ethers and poly(acrylic acid), Carbohydr. Polym. 215 (2019) 58–62, https://doi.org/10.1016/j.carbpol.2019.03.066.

[24] N. Kébir, M. Benoit, C. Legrand, F. Burel, Non-isocyanate thermoplastic polyureas (NIPUreas) through a methyl carbamate metathesis polymerization, Eur. Polym. J. 96 (2017) 87–96, https://doi.org/10.1016/j.eurpolymj.2017.08.046.

[25] C. Carré, Y. Ecochard, S. Caillol, L. Avérous, From the synthesis of biobased cyclic carbonate to polyhydroxyurethanes: a promising route towards renewable non-isocyanate polyurethanes, ChemSusChem. 12 (2019) 3410–3430, https://doi.org/10.1002/cssc.201900737.

[26] A. Bossion, R.H. Aguirresarobe, L. Irusta, D. Taton, H. Cramail, E. Grau, D. Mecerreyes, C. Su, G. Liu, A.J. Müller, H. Sardon, Unexpected synthesis of segmented poly(hydroxyurea-urethane)s from dicyclic carbonates and diamines by organocatalysis, Macromolecules. 51 (2018) 5556–5566, https://doi.org/10.1021/acs.macromol.8b00731.

[27] H.I. Mao, C.W. Chen, H.C. Yan, S.P. Rwei, Synthesis and characteristics of nonisocyanate polyurethane composed of bio-based dimer diamine for supercritical CO2 foaming applications, J. Appl. Polym. Sci. 139 (2022) e52841.
[28] K. Breul, S. Seiffert, Amphiphilic poly(ether urethanes) carrying associative terpyridine side groups with controlled spacing, Polym. Chem. 12 (2021) 2305–2316, https://doi.org/10.1039/D1PY00121C.
[29] K. Jiang, W. Chen, X. Liu, Y. Wang, D. Han, Q. Zhang, Effect of bio-based polyols and chain extender on the microphase separation structure, mechanical properties and morphology of rigid polyurethane foams, Eur. Polym. J. 179 (2022), 111572, https://doi.org/10.1016/J.EURPOLYMJ.2022.111572.
[30] A. Bukowczan, E. Hebda, M. Czajkowski, K. Pielichowski, The synthesis and properties of liquid crystalline polyurethanes, chemically modified by polyhedral oligomericsilsesquioxanes, Molecules. 24 (2019) 4013, https://doi.org/10.3390/molecules24224013.
[31] Y. Eom, S.M. Kim, M. Lee, H. Jeon, J. Park, E.S. Lee, S.Y. Hwang, J. Park, D.X. Oh, Mechano-responsive hydrogen-bonding array of thermoplastic polyurethane elastomer captures both strength and self-healing, Nat. Commun. 12 (2021) 1–11, https://doi.org/10.1038/s41467-021-20931-z.
[32] Y. Zeng, Y. Chen, D. Sha, Y. Wu, R. Qiu, W. Liu, Highly stretchable fatty acid chain-dangled thermoplastic polyurethane elastomers enabled by h-bonds and molecular chain entanglements, ACS Sustain. Chem. Eng. 10 (2022) 11524–11532, https://doi.org/10.1021/acssuschemeng.2c02877.
[33] Z. Wang, Z. Liu, Z. Gao, X. Li, B. Eling, E. Pöselt, E. Schander, Z. Wang, Structure transition of aliphatic m,6-Polyurethane during heating investigated using in-situ WAXS, SAXS, and FTIR, Polymer (guildf). 254 (2022), 125072, https://doi.org/10.1016/j.polymer.2022.125072.
[34] D.J. Skrovanek, P.C. Painter, M.M. Coleman, Hydrogen Bonding in Polymers. 2. Infrared Temperature Studies of Nylon 11, Macromolecules. 19 (1986) 699–705. https://doi.org/10.1021/ma00157a037.
[35] E.S. Feldblum, I.T. Arkin, Strength of a bifurcated H bond, Proc. Natl. Acad. Sci. u. s. a. 111 (2014) 4085–4090, https://doi.org/10.1073/pnas.1319827111.
[36] H.Y. Liao, S.Y. Chu, Hydrogen bond acceptor capability of carbonyl π-electrons—case study of the hydrogen-bonded urea dimer, New J. Chem. 27 (2003) 421–424, https://doi.org/10.1039/B202440N.
[37] X.H. Chen, J. Yu, L.Z. Gong, The role of double hydrogen bonds in asymmetric direct aldol reactions catalyzed by amino amide derivatives, Chem. Commun. 46 (2010) 6437–6448, https://doi.org/10.1039/C0CC00754D.
[38] D.P. Queiroz, M.N. De Pinho, C. Dias, ATR-FTIR studies of poly(propylene oxide)/polybutadiene Bi-soft segment urethane/urea membranes, Macromolecules. 36 (2003) 4195–4200, https://doi.org/10.1021/ma034032t.
[39] X.Z. Li, B. Walker, A. Michaelides, Quantum nature of the hydrogen bond, Proc. Natl. Acad. Sci. u. s. a. 108 (2011) 6369–6373, https://doi.org/10.1073/pnas.1016653108.
[40] M.M. Deshmukh, S.R. Gadre, Molecular tailoring approach for the estimation of intramolecular hydrogen bond energy, Molecules. 26 (2021) 2928, https://doi.org/10.3390/molecules26102928.
[41] M.S. Bradley, J.H. Krech, High-pressure raman spectra of the acetone carbonyl stretch in acetone-methanol mixtures, J. Phys. Chem. 97 (1993) 575–580, https://doi.org/10.1021/j100105a009.
[42] R.G.M. Van Der Sman, Predictions of glass transition temperature for hydrogen bonding biomaterials, J. Phys. Chem. b. 117 (2013) 16303–16313, https://doi.org/10.1021/jp408184u.
[43] F. Varnik, J. Baschnagel, K. Binder, Reduction of the glass transition temperature in polymer films: A molecular-dynamics study, Phys. Rev. e. 65 (2002), 021507, https://doi.org/10.1103/PhysRevE.65.021507.
[44] M. Vallance, A.S. Yeung, S.L. Cooper, A dielectric study of the glass transition region in segmented polyether-urethane copolymers, Colloid Polym. Sci. Polym. Sci. 261 (1983) 541–554, https://doi.org/10.1007/BF01526619.
[45] K.N. Raftopoulos, B. Janowski, L. Apekis, K. Pielichowski, P. Pissis, Molecular mobility and crystallinity in polytetramethylene ether glycol in the bulk and as soft component in polyurethanes, Eur. Polym. J. 47 (2011) 2120–2133, https://doi.org/10.1016/j.eurpolymj.2011.07.020.
[46] J.F. Mano, J.L. Gómez Ribelles, N.M. Alves, M. Salmerón Sanchez, Glass transition dynamics and structural relaxation of PLLA studied by DSC: Influence of crystallinity, Polymer (guildf). 46 (2005) 8258–8265, https://doi.org/10.1016/j.polymer.2005.06.096.
[47] J. Ke, X. Li, S. Jiang, C. Liang, J. Wang, M. Kang, Q. Li, Y. Zhao, Promising approaches to improve the performances of hybrid non-isocyanate polyurethane, Polym. Int. 68 (2019) 651–660, https://doi.org/10.1002/pi.5746.
[48] J.D. Wolfgang, B.T. White, T.E. Long, Non-isocyanate Polyurethanes from 1,1′-Carbonyldiimidazole: A Polycondensation Approach, (2021). https://doi.org/10.1002/marc.202100163.
[49] J. Dong, B. Liu, H. Ding, J. Shi, N. Liu, B. Dai, I. Kim, Bio-based healable non-isocyanate polyurethanes driven by the cooperation of disulfide and hydrogen bonds, Polym. Chem. 11 (2020) 7524–7532, https://doi.org/10.1039/D0PY01249A.
[50] V. Schimpf, B.S. Ritter, P. Weis, K. Parison, R. Mülhaupt, High purity limonene dicarbonate as versatile building block for sustainable non-isocyanate polyhydroxyurethane thermosets and thermoplastics, Macromolecules. 50 (2017) 944–955, https://doi.org/10.1021/acs.macromol.6b02460.
[51] G. Beniah, K. Liu, W.H. Heath, M.D. Miller, K.A. Scheidt, J.M. Torkelson, Novel thermoplastic polyhydroxyurethane elastomers as effective damping materials over broad temperature ranges, Eur. Polym. J. 84 (2016) 770–783, https://doi.org/10.1016/J.EURPOLYMJ.2016.05.031.
[52] S. Weyand, H. Blattmann, V. Schimpf, R. Mülhaupt, R. Schwaiger, Structure-property-glass transition relationships in non-isocyanate polyurethanes investigated by dynamic nanoindentation, Mater. Res. Express. 3 (2016), 075019, https://doi.org/10.1088/2053-1591/3/7/075019.
[53] T. Chen, C. Su, Y. Zeng, Y. Chen, R. Qiu, W. Liu, Effects of hydrogen bonds on soybean oil-based thermosets and their bamboo fibers composites, Compos. Commun. 33 (2022), 101231, https://doi.org/10.1016/J.COCO.2022.101231.
[54] N.R. Choudhury, A.G. Kannan, N.K. Dutta, Novel nanocomposites and hybrids for lubricating coating applications, Tribol. Interface Eng. Ser. 55 (2008) 501–542, https://doi.org/10.1016/S1572-3364(08)55021-X.
[55] A. Gasperini, G.J.N. Wang, F. Molina-Lopez, H.C. Wu, J. Lopez, J. Xu, S. Luo, D. Zhou, G. Xue, J.B.H. Tok, Z. Bao, Characterization of hydrogen bonding formation and breaking in semiconducting polymers under mechanical strain, Macromolecules. 52 (2019) 2476–2486, https://doi.org/10.1021/acs.macromol.9b00145.
[56] K.P. Menard, N.R. Menard, Dynamic Mechanical Analysis, 3rd ed., CRC Press, Boca Raton, 2020.
[57] O.V. Startsev, Y.M. Vapirov, M.P. Lebedev, A.K. Kychkin, Comparison of glass-transition temperatures for epoxy polymers obtained by methods of thermal analysis, Mech. Compos. Mater. 56 (2020) 227–240, https://doi.org/10.1007/s11029-020-09875-5.
[58] C.A. Gracia-Fernández, S. Gómez-Barreiro, J. López-Beceiro, J. Tarrío Saavedra, S. Naya, R. Artiaga, Comparative study of the dynamic glass transition temperature by DMA and TMDSC, Polym. Test. 29 (2010) 1002–1006, https://doi.org/10.1016/j.polymertesting.2010.09.005.
[59] N. Padhye, A. Vallabh, Deformation-induced bonding of polymer films below the glass transition temperature, J. Appl. Polym. Sci. 138 (2021) 50934, https://doi.org/10.1002/app.50934.
[60] A. Asif, W. Shi, X. Shen, K. Nie, Physical and thermal properties of UV curable waterborne polyurethane dispersions incorporating hyperbranched aliphatic polyester of varying generation number, Polymer (guildf). 46 (2005) 11066–11078, https://doi.org/10.1016/j.polymer.2005.09.046.
[61] P. Somdee, T. Lassú-Kuknyó, C. Kónya, T. Szabó, K. Marossy, Thermal analysis of polyurethane elastomers matrix with different chain extender contents for thermal conductive application, J. Therm. Anal. Calorim. 138 (2019) 1003–1010, https://doi.org/10.1007/S10973-019-08183-Y.
[62] M. Wübbenhorst, J. van Turnhout, Analysis of complex dielectric spectra. I. One-dimensional derivative techniques and three-dimensional modelling, J. Non. Cryst. Solids. 305 (2002) 40–49, https://doi.org/10.1016/S0022-3093(02)01086-4.
[63] F. Kremer, A. (Andreas) Schönhals, Broadband Dielectric Spectroscopy, 1st ed., Springer Berlin, Heidelberg, 2002. https://doi.org/10.1007/978-3-642-56120-7.
[64] S. Havriliak, S. Negami, A complex plane representation of dielectric and mechanical relaxation processes in some polymers, Polymer (guildf). 8 (1967) 161–210, https://doi.org/10.1016/0032-3861(67)90021-3.
[65] S. Havriliak, S. Negami, A complex plane analysis of α-dispersions in some polymer systems, J. Polym. Sci. Part C Polym. Symp. 14 (1966) 99–117, https://doi.org/10.1002/polc.5070140111.
[66] D. Fragiadakis, J. Runt, Molecular dynamics of segmented polyurethane copolymers: in fluence of soft segment composition, Macromolecules. 46 (2013) 4184–4190, https://doi.org/10.1021/ma4006395.
[67] K.N. Raftopoulos, I. Łukaszewska, C. Bujalance Calduch, P. Stachak, S. Lalik, E. Hebda, M. Marzec, K. Pielichowski, Hydration and glass transition of hybrid non-isocyanate polyurethanes with POSS inclusions, Polymer (guildf). 253 (2022), 125010, https://doi.org/10.1016/j.polymer.2022.125010.
[68] S. Kosma, K. Raftopoulos, P. Pissis, A. Strachota, L. Matějka, F. Ribot, J. Nedbal, Molecular mobility of stannoxane modified epoxy resins, J. Nanostructured Polym. Nanocomposites. 3 (4) (2007) 144–156.
[69] E. Schlosser, A. Schönhals, Relation between main- and normal-mode relaxation. A dielectric study on poly (propyleneoxide), in: B. Ewen, E.W. Fischer, G. Fytas (Eds.), Appl. Scatt. Methods to Dyn. Polym. Syst., Steinkopff, Darmstadt, 1993: pp. 158–161. https://doi.org/10.1007/BFb0116484.
[70] A. Boersma, J. van Turnhout, M. Wübbenhorst, Dielectric characterization of a thermotropic liquid crystalline copolyesteramide: 1. Relaxation peak assignment, Macromolecules. 31 (1998) 7453–7460, https://doi.org/10.1021/MA9716138.
[71] J. Mijovic, M. Sun, Y. Han, Normal and segmental mode dynamics of end-functionalized poly (propylene oxide) by dielectric relaxation spectroscopy and dynamic mechanical spectroscopy, Macromolecules. 35 (2002) 6417–6425, https://doi.org/10.1021/ma020293b CCC.
[72] H. Vogel, Das Temperaturabhaengigkeitsgesetz der Viskositaet von Fluessigkeiten, Phys. z. 22 (1921) 645–646.
[73] G.S. Fulcher, Analysis of recent measurements of the viscosity of glasses, J. Am. Ceram. Soc. 8 (1925) 339–355, https://doi.org/10.1111/j.1151-2916.1925.tb16731.x.
[74] G. Tammann, W. Hesse, Temperature dependence of viscosity of melted supercooled liquids, Z. Anorg. Allgem. Chem. 156 (1926) 245–247.
[75] C.A. Angell, Relaxation in liquids, polymers and plastic crystals-strong/fragile patterns and problems, J. Non. Cryst. Solids. 131 (1991) 13–31, https://doi.org/10.1016/0022-3093(91)90266-9.
[76] A. Shundo, M. Aoki, S. Yamamoto, K. Tanaka, Cross-linking effect on segmental dynamics of well-defined epoxy resins, Macromolecules. 54 (2021) 5950–5956, https://doi.org/10.1021/acs.macromol.1c00513.
[77] K.N. Raftopoulos, C. Pandis, L. Apekis, P. Pissis, B. Janowski, K. Pielichowski, J. Jaczewska, Polyurethane-POSS hybrids: Molecular dynamics studies, Polymer (guildf). 51 (2010) 709–718, https://doi.org/10.1016/j.polymer.2009.11.067.